American Mineralogist, Volume 63, pages 378–393, 1978

The low-temperature stability of andradite in C–O–H fluids

BRUCE E. TAYLOR[1] AND JUHN G. LIOU

Tuttle-Jahns Laboratory for Experimental Petrology and
Department of Geology, Stanford University
Stanford, California 94305

Abstract

The low-temperature stability of andradite was experimentally investigated as a function of temperature, X_{CO_2} and f_{O_2} at constant P_{fluid} of 2000 bars. Experimental results indicate that the reaction 3 quartz + 3 calcite + ¼ hematite + ½ magnetite + ⅛ O_2 = andradite + 3 CO_2 occurs at T = 550 ± 10°C at X_{CO_2} = 0.22, 596 ± 8°C at X_{CO_2} = 0.5, and 640 ± 10°C at X_{CO_2} = 1.0. From these experimental data, the standard (298°K, 1 bar) Gibbs free energy of formation of andradite ($G^0_{f,Ad}$) is −1293.44 ± 1.2 kcal/gfw, and the enthalpy ($H^0_{f,Ad}$) is −1377.48 ± 1.2 kcal/gfw. These values are slightly less negative than those for $G^0_{f,Ad}$ and $H^0_{f,Ad}$ calculated from data of Gustafson (1974). Mean values for $G^0_{f,Ad}$ and $H^0_{f,Ad}$ derived from Gustafson's experiments and the present results are, respectively, −1297.80 kcal/gfw and −1382.13 kcal/gfw. The standard entropy of formation of andradite ($S^0_{f,Ad}$) is −282 ± 4 gb/gfw, and the Third Law entropy (S^0) is 68.2 ± 3 gb/gfw, which is close to the oxide sum estimate of 69.0 gb/gfw.

The experimental data for the low-temperature stability of andradite plus other pertinent data on the stabilities of wollastonite, hedenbergite (calculated), clinozoisite (zoisite), epidote, and grossular provide T–X_{CO_2}–f_{O_2}–P_{fluid} relations which delineate physical-chemical conditions for Ca–Fe–Al–Si skarn formation.

Relative to the stability field of grossular in C–O–H fluids (Gordon and Greenwood, 1971), andradite is stable with fluids richer in CO_2 at a given temperature and pressure for all values of f_{O_2}, although the temperatures of reactions which delineate the stability field of andradite are sensitive to slight changes in either X_{CO_2}, f_{O_2}, or both. Like grossular, andradite is stable to lower temperatures with H_2O-rich fluids. Addition of Fe^{3+} to grossular extends the thermal stability limits of grandite plus quartz to both higher and lower temperatures. In natural systems, simple retrograde carbonation of grandite may not occur if the fluid is sufficiently H_2O-rich to stabilize epidote.

Introduction

Andradite, or andradite-rich garnet, is a principal mineral in many contact-metasomatic skarns. Andradite-bearing skarns have often been mined as ore deposits of W and/or Cu (*e.g.* Kerr, 1946). Hence, an understanding of the stability of andradite may help to elucidate the physical and chemical parameters which characterize the formation of skarn. From its chemical composition ($Ca_3Fe_2Si_3O_{12}$) and its occurrence at or near contacts between igneous rocks and calcite-rich rocks, it is apparent that many mineral reactions involving andradite take place in fluids containing carbon, oxygen, and hydrogen, and are simultaneously both decarbonation and redox reactions. Minor variations in fluid composition or f_{O_2}, or both, may therefore markedly influence the temperature and pressure at which these reactions take place.

Burt (1971a,b,c; 1972; 1974) developed topological relations among mineral reactions in the system Ca–Fe–Si–C–O–H for unspecified values of T, P_{fluid}, f_{O_2}, and various chemical potentials consistent with phase relations observed in skarns. Stability relations of andradite in the system Ca–Fe–Si have been extensively investigated (*e.g.* Kurshakova, 1968, 1970, 1971; Huckenholz and Yoder, 1971; Gustafson, 1971, 1974; Liou, 1974). The results of experiments at 1 atm by Holdaway (1972) suggest that grandite garnet closely approximates an ideal solution, and that the

[1] Present address: Department of Geology, University of California, Davis, California 95616.

0003–004X/78/0304–0378$02.00

addition of andradite to grandite garnet raises the upper thermal stability limit of the garnet. However, except for a few reconnaissance experiments by Shoji (1975) and Gustafson (1971), the low-temperature stability of andradite defined by the reaction:

$$3\,SiO_2 + 3CaCO_3 + Fe_2O_3 = Ca_3Fe_2Si_3O_{12} + 3CO_2$$
quartz calcite hematite andradite

has not been experimentally investigated. The effect of CO_2 on the stability of andradite is petrologically significant, since the above decarbonation reaction defines the low-temperature stability limit of andradite garnet in natural skarn. Further, CO_2 and H_2O are the dominant fluid species in many skarn-forming processes. Because iron is present in the system, oxygen fugacity is an additional parameter governing not only the temperature and stoichiometry of the above equilibrium, but also the nature of the iron-oxide phase present. The low-temperature stability limit of andradite in C–O–H fluids at f_{O_2} defined by the HM buffer was investigated in this study, and the experimental results and their petrologic applications are described below.

A plot of andradite and some other phases in the system Ca–Fe–Si–C–O–H is shown in Figure 1. The abbreviations and chemical compositions of synthetic phases and oxygen buffers referred to in other figures and in the text are given in Table 1. Chemical reactions and their abbreviations, referred to by number in the text, are given in Table 2.

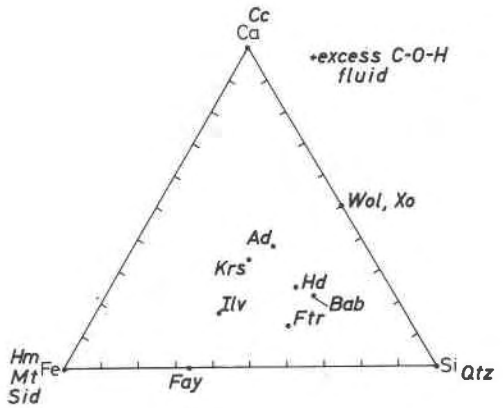

Fig. 1. Chemical compositions of several important crystalline phases in the system Ca–Fe–Si–C–O–H projected onto the Ca–Fe–Si plane.

Experiments

Starting materials

Synthetic andradite: Andradite ($Ca_3Fe_2Si_3O_{12}$) was readily synthesized with 100 percent yield from a nitrate gel (Luth and Ingamells, 1965) of andradite composition at 700° to 750°C, 2 kbar P_{fluid}. Honey-colored andradite crystals ($a = 12.061 \pm 0.03$A) grew as large as 130 μm in synthesis runs of 14 days duration.

Natural quartz: Natural quartz from a clear euhedral crystal was used as part of the low-temperature, andradite-equivalent assemblage. The quartz was crushed and washed in warm dilute HNO_3 prior to use.

Calcite and iron oxides: Baker-analyzed reagent-grade $CaCO_3$, Fe_2O_3, and Fe_3O_4 were used in the low-temperature, andradite-equivalent assemblage.

C–O and C–O–H fluids: Commercial tank CO_2 was used as both the pressure medium and the source of CO_2 in experiments with fluids in the system C–O (Harker and Tuttle, 1955). For C–O–H fluids with $X_{CO_2} = 0.5$, oxalic acid dihydrate was used (Holloway *et al.*, 1968), whereas fluids with $X_{CO_2} < 0.5$ were produced from oxalic acid dihydrate plus warm (*i.e.* CO_2-free) distilled water.

The starting mixture consisted of sub-equal

Table 1. Abbreviations and compositions for synthetic phases and oxygen buffer assemblages

Ad	= Andradite, $Ca_3Fe^{3+}_2Si_3O_{12}$	Ilv	= Ilvaite, $CaFe_2{}^{2+}Fe^{3+}Si_2O_3(OH)$
An	= Anorthite, $CaAl_2Si_2O_8$	Mt	= Magnetite, Fe_3O_4
Cc	= Calcite, $CaCO_3$	Ps	= Pistacite, $Ca_2Fe_3Si_3O_{12}(OH)$
Ep	= Epidote, $Ca_2Al_{2+x}Fe_{1-x}Si_3O_{12}(OH)$	Qtz	= Quartz, SiO_2
Fay	= Fayalite, Fe_2SiO_4	Sid	= Siderite, $FeCO_3$
Ftr	= Ferrotremolite, $Ca_2Fe_5{}^{2+}Si_8O_{22}(OH)_2$	Wol	= Wollastonite, $CaSiO_3$
Gd	= Grandite Garnet, $Ca_3Al_xFe_{2-x}Si_3O_{12}$	Xo	= Xonotolite, $Ca_6Si_6O_{17}(OH)_2$
Gr	= Grossular, $Ca_3Al_2Si_3O_{12}$	Zo	= Zoisite, $Ca_2Al_3Si_3O_{12}(OH)$
Hd	= Hedenbergite, $CaFeSi_2O_6$	HM	= Hematite-Magnetite
Hm	= Hematite, Fe_2O_3	NNO	= Nickel-Nickel Oxide

Table 2. Reactions and their abbreviations cited in text and figures

No.	Reaction	Abbreviation	Reference
1	$3SiO_2 + 3CaCO_3 + 1/4Fe_2O_3 + 1/2Fe_3O_4 + 1/8O_2 = Ca_3Fe_2Si_3O_{12} + 3CO_2$ (Qtz, Cc, Hm, Mt; Ad)	Qtz-Cc-Hm-Mt-Ad	This paper
2	$Ca_3Fe_2Si_3O_{12} = 3CaSiO_3 + 2/3Fe_3O_4 + 1/6O_2$	Ad-Wol-Mt	Gustafson (1971, 1974)
3	$Ca_3Fe_2Si_3O_{12} + 2SiO_2 = 2CaFeSi_2O_6 + CaSiO_3 + 1/2O_2$ (Ad, Qtz, Hd, Wol)	Ad-Qtz-Hd-Wol	Liou (1974)
4	$CaFeSi_2O_6 + O_2 = 1/3Ca_3Fe_2Si_3O_{12} + SiO_2 + 1/9Fe_3O_4$ (Hd, Ad, Qtz, Mt)	Hd-Ad-Qtz-Mt	Gustafson (1974)
5	$CaFeSi_2O_6 = CaSiO_3 + Fe + SiO_2 + 1/2O_2$ (Hd, Wol, Qtz)	Hd-Wol-I-Qtz	Kurshakova and Avetisyan (1974)
6	$SiO_2 + CaCO_3 = CaSiO_3 + CO_2$ (Qtz, Cc, Wol)	Qtz-Cc-Wol	Greenwood (1967a)
7	$CaAl_2Si_2O_8 + SiO_2 + 2CaCO_3 = Ca_3Al_2Si_3O_{12} + 2CO_2$ (An, Qtz, Cc, Gr)	An-Qtz-Cc-Gr	Gordon and Greenwood (1971)
8	$Ca_3Al_2Si_3O_{12} + SiO_2 = CaAl_2Si_2O_8 + 2CaSiO_3$ (Gr, Qtz, An, Wol)	Gr-Qtz-An-Wol	Newton (1966)
9	$9SiO_2 + 9CaCO_3 + 2Fe_3O_4 + 1/2O_2 = 3Ca_3Fe_2Si_3O_{12} + 9CO_2$ (Qtz, Cc, Mt; Ad)	Qtz-Cc-Mt-Ad	This paper
10	$2CaFeSi_2O_6 + CaCO_3 + 1/2O_2 = Ca_3Fe_2Si_3O_{12} + SiO_2 + CO_2$ (Hd, Cc; Ad, Qtz)	Hd-Cc-Ad-Qtz	Liou (1974)
11	$6SiO_2 + 3CaCO_3 + Fe_3O_4 = 3CaFeSi_2O_6 + 3CO_2 + 1/2O_2$ (Qtz, Cc, Mt, Hd)	Qtz-Cc-Mt-Hd	This paper
12	$4Ca_2Al_3Si_3O_{12}(OH) + SiO_2 = 5CaAl_2Si_2O_3 + Ca_3Al_2Si_3O_{12} + 2H_2O$ (Zo, Qtz; An, Gr)	Zo-Qtz-An-Gr	Gordon and Greenwood (1971)
13	$2Ca_2Al_3Si_3O_{12}(OH) + 3SiO_2 + 5CaCO_3 = 3Ca_3Al_2Si_3O_{12} + H_2O + 5CO_2$ (Zo, Qtz, Cc; Gr)	Zo-Qtz-Cc-Gr	Gordon and Greenwood (1971)
14	$2Ca_2Al_3Si_3O_{12}(OH) + CO_2 = 3CaAl_2Si_2O_8 + CaCO_3 + H_2O$ (Zo; An, Cc)	Zo-An-Cc	Johannes and Orville (pers. commun., 1974); Gordon and Greenwood (1971)
15	$Epidote_{ss} + Quartz = Grandite_{ss} + Magnetite_{ss} + Anorthite + Quartz + H_2O + O_2$	Ep-Qtz-Gd-Mt_{ss}-An	(see text)
16	$Epidote_{ss} + Quartz + Calcite = Grandite + CO + H_2O$	Ep-Qtz-Cc-Gd	(see text)
17	$Epidote_{ss} + CO_2 = Grandite + Calcite + H_2O$	Ep-Gd-Cc	(see text)

amounts of synthetic andradite and its low-temperature equivalent assemblage of quartz, calcite, and iron oxide ground together to $<5\mu$m. Approximately 30 mg of this mixture was used in each experiment, as described below.

Methods

Experiments were performed by placing one or two charge capsules in conventional hydrothermal cold-seal pressure vessels and holding them at desired temperatures and pressures for at least three weeks. Runs were quenched to room temperature within several minutes using an air blower. External Cr–Al thermocouples, calibrated relative to the temperature within the vessel, were used to record temperature during the runs. Temperature uncertainties for each experiment, including temperature gradients and control precision, are typically ± 5°C. Fluid pressure was continuously monitored on individual Bourdon-tube gauges which were calibrated against a 50,000 psi Heise gauge. Pressure uncertainties are approximately ± 30 bars. Two different types of experiments were undertaken in the present study, as described below.

Experiments in C–O fluids: In these experiments, pure CO_2 was used for the pressure medium as well as for the source of CO_2 for the reaction. Oxygen fugacity was controlled by the presence of Hm and Mt in the outer (buffer) capsule (silver tubing, 5 mm O.D.) and in the inner (charge) capsule (silver tubing, 3 mm O.D.). Both capsules were crimped at each end to permit access of CO_2 to the charge material during the experiment. Optical examination of the HM buffer after each experiment was generally sufficient to determine that both phases were present. Finding both Hm and Mt in the run products provided additional assurance that the oxygen fugacity was that defined by the HM buffer during the experiment. The experimental arrangement was otherwise similar to that described by French (1971). Reaction rates in pure-CO_2 experiments are extremely sluggish (*e.g.* Harker and Tuttle, 1955); runs of 3-months duration, even at temperatures of 500–600°C, did not show any conclusive reaction. Therefore, addition of a tiny drop ($\ll$ 1 mg) of H_2O to the charge was necessary in order to increase the reaction rate sufficiently in the nearly pure C–O fluid ($X_{CO_2} \geq 0.95$), so that a reaction could be detected in experiments of nearly 2 months duration.

Experiments in C–O–H fluids: The second type of experiment employed the use of C–O–H fluids and a capsule arrangement similar to that described by Eugster (1957). Again, about 30 mg of the starting mixture and 30 mg of oxalic acid dihydrate ± H_2O were sealed in a $Ag_{30}Pd_{70}$ capsule (3 mm O.D.) which was then loaded into the buffer capsule (silver or gold tubing, 5 mm O.D.) containing hematite and magnetite plus 30 mg of H_2O. The pressure medium was either H_2O or CO_2. For experiments at f_{H_2} defined by the hematite–magnetite–OH buffer, H_2O and CO_2 are the principal species in the C–O–H charge fluid (Eugster and Skippen, 1967; Holloway *et al.*, 1968). Because sufficient fluid was loaded into the charge capsule, the CO_2 released from decomposition of calcite did not have a significant effect on the initial fluid composition. At the end of each experiment, the composition of the fluid in the charge was determined gravimetrically (for details see Taylor, 1976), with a resulting uncertainty for X_{CO_2} believed to be ± 0.02. A slight shift in the fluid composition was found in some experiments, due to the formation of calcite at the expense of andradite. Changes in the fluid composition detected after the experiment also indicated the direction of the reaction.

Run products were identified optically and with X-ray diffraction. The direction of reaction was determined by comparison of peak-height ratios of andradite to quartz in the charge material with those ratios measured in the starting mixture. Several 0.5° 2θ per minute scans of a powder mount held in several different orientations gave reproducible results. In each experiment using a C–O–H fluid, the reaction had proceeded sufficiently in three weeks to permit a confident determination of the direction of reaction.

Note that in these experiments oxygen fugacity was not buffered in the usual way, through the dissociation of H_2O within the charge under controlled f_{H_2}, T, and P (Eugster, 1957; Shaw, 1963), but rather internally by the reaction:

$$3\ Fe_2O_3 = 2\ Fe_3O_4 + 1/2\ O_2.$$

We chose to externally control f_{H_2}, however, to insure that f_{O_2} within the charge would not be above that of the HM buffer, as might have resulted from the large amounts of fluid used.

Experimental results

Experimental run data at 2 kbar P_{fluid} for the reaction:

$$\underset{\text{quartz}}{3\ SiO_2} + \underset{\text{calcite}}{3\ CaCO_3} + \underset{\text{hematite}}{1/4\ Fe_2O_3} + \underset{\text{magnetite}}{1/2\ Fe_3O_4} + 1/8\ O_2 = \underset{\text{andradite}}{Ca_3Fe_2Si_3O_{12}} + 3CO_2 \quad (1)$$

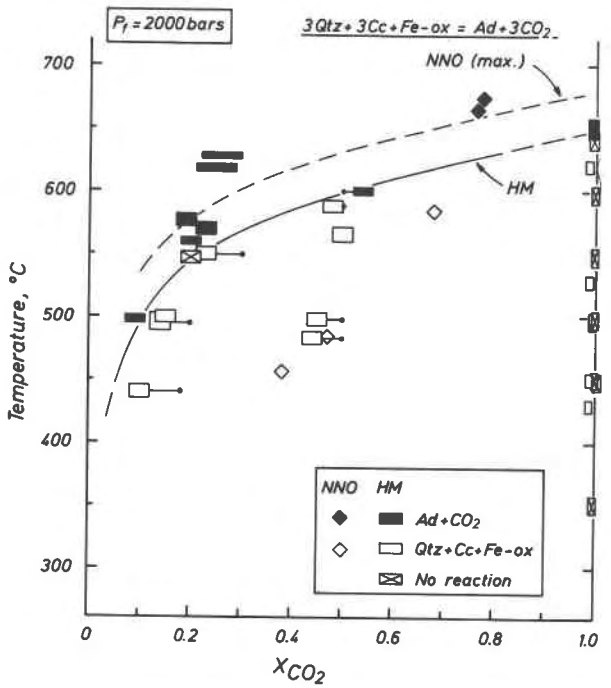

Fig. 2. Experimentally-determined T–X_{CO_2} diagram for the reaction 3 Qtz + 3 Cc + FeOx = Ad + 3 CO_2. The magnitude of experimental error is indicated by the size of the rectangles (HM buffer only). The initial X_{CO_2} in the experimental fluid (dots) and direction and magnitude of shift in fluid composition due to crystallization of calcite (indicated by bars) are shown for runs in which a change in fluid composition was detected after the run. Diamond-shaped symbols are reconnaissance run data of Gustafson (1971). The dashed line indicates the maximum possible temperature for the reaction with oxygen fugacity determined by the NNO buffer.

in C–O and C–O–H fluids are listed in Table 3 and are plotted on a T–X_{CO_2} diagram in Figure 2. Both the initial values of X_{CO_2} in the experimental fluid and the values of X_{CO_2} which were measured after each experiment are shown in Figure 2. For runs in which a change in X_{CO_2} was detected after the experiment, a point and a connecting bar are used in the T–X_{CO_2} diagram to indicate, respectively, the initial X_{CO_2} in the charge and the direction and magnitude of change in X_{CO_2} during the experiment. Closely-bracketed equilibrium temperatures for reaction (1) at P_{fluid} = 2000 bars are 550 ± 10°C at X_{CO_2} = 0.22, 596 ± 8°C at X_{CO_2} = 0.5, and 640 ± 10°C at $X_{CO_2} \simeq 1.0$.

Several runs in which either the charge capsule or both the buffer and charge capsules leaked during the experiment are listed in Table 3, if the f_{O_2} and fluid composition during the experiment could be determined. In experiments where only the charge capsule leaked, the above reaction would have occurred in the system andradite plus excess iron oxide, and the uncertainty in X_{CO_2} in these experiments (*e.g.* run no. 74-96) is slightly greater than in normal runs. The runs which leaked are listed for reference only.

An initial attempt to reverse reaction (1), *i.e.*, to form the low-temperature assemblage of quartz, calcite, and iron oxide from andradite, was made in a pure C–O fluid. The only water present to act as a catalyst was the surface moisture absorbed on the buffer and charge materials. The rate of reaction in these experiments was so slow that no breakdown of andradite to quartz, calcite, and iron oxide was detected in experiments of up to three months duration at 500° to 600°C. However, with the addition of a drop of H_2O to the charge, the rate of reaction was significantly increased. Andradite was grown at the expense of the low-temperature assemblage at 649°C (run no. SM-1, Table 3) after 22 days. No reaction was observed at 639°C (run no. SM-2) for the same length of time. From these data and the results described below, we conclude that the equilibrium temperature for the above reaction at X_{CO_2} = 1.0 is 640 ±10°C at 2000 bars P_{fluid}.

In contrast to the experiments in pure C–O fluids, a reaction was readily detected after three weeks in runs made with C–O–H fluids. The decomposition of andradite was clearly indicated, not only by changes in the relative peak-height ratios in X-ray diffraction patterns of andradite and quartz but also by a decrease in X_{CO_2} in the experimental fluid due to the formation of calcite (see, for example, run no. 74-175, Table 3). A relative increase in the grain size of andradite, especially where euhedral crystals of andradite were seen to enclose hematite, supported the X-ray diffraction criterion for synthesis of andradite in the decarbonation reaction.

In several instances where both the charge and buffer capsules leaked during the experiments using CO_2 as the pressure medium (*e.g.* run no. 74-83), the fluid composition changed from an initial relatively low value of X_{CO_2} to values greater than 0.95. Unlike experiments using a pure C–O fluid, a reaction was readily detected in those experiments which leaked, and the results are consistent with those of experiments using controlled C–O–H fluids. The decomposition of andradite took place in the fluids with X_{CO_2} =0.95 at temperatures ranging from 430°C (run no. 74-83, Table 3) to 620°C (run no. 74-97).

The reversed-run data from experiments using C–O–H fluids indicate that the breakdown temperature of andradite to quartz, calcite, and iron oxide is quite sensitive to variation in X_{CO_2} in H_2O-rich fluids (*i.e.* $X_{CO_2} < 0.5$; see Fig. 2). The apparently steep T–X_{CO_2}

Table 3. Run data for the reaction 3Qtz + 3Cc + 1/4 Hm + 1/2 Mt + 1/8 O_2 = Ad+3CO_2 at P_{fluid} = 2000 bars, and f_{O_2} defined by the HM buffer

Run No.	Duration (hrs)	T°(C)	--- X_{CO_2} --- Initial	Final	Condensed Run Products†	Remarks
Crimped capsule runs, C-O fluid						
74-06	340	352 ± 7	1.0	1.0	Ad + Qtz + Cc + Fe-Ox	No reaction
74-05	340	450 ± 7	1.0	1.0	Ad + Qtz + Cc + Fe-Ox	"
74-33	1267	450 ± 7	1.0	1.0	Sid + Mt	HM buffer exhausted, f_{O_2} below HM
74-39	1979	450 ± 7	1.0	1.0	Ad + Qtz + Cc + Fe-Ox	No reaction
74-08	500	498 ± 7	1.0	1.0	Ad + Qtz + Cc + Fe-Ox	" "
74-35	2844	498 ± 7	1.0	1.0	Ad + Qtz + Cc + Fe-Ox	" "
74-07	340	548 ± 7	1.0	1.0	Ad + Qtz + Cc + Fe-Ox	" "
74-37	1954	597 ± 7	1.0	1.0	Ad + Qtz + Cc + Fe-Ox	" "
Sealed capsule runs, C-O-H fluid						
74-83*	730	430 ± 7	0.50	> 0.95	(Ad)+ Qtz + Cc + Fe-Ox	Charge & buffer capsules leaked
74-81*	730	451 ± 5	0.50	> 0.95	(Ad)+ Qtz + Cc + Fe-Ox	" " " "
Ad-3	1332	454 ± 7	0.18	0.11	(Ad)+ Qtz + Cc + Fe-Ox	
74-77	840	483 ± 7	0.50	0.44	(Ad)+ Qtz + Cc + Fe-Ox	
74-175	671	495 ± 7	0.20	0.14	(Ad)+ Qtz + Cc + Fe-Ox	
74-67	840	498 ± 5	0.50	0.45	(Ad)+ Qtz + Cc + Fe-Ox	
74-153	612	498 ± 3	0.09	0.09	(Qtz + Cc + Fe-Ox)	
74-151	671	500 ± 5	0.15	0.15	(Ad)+ Qtz + Cc + Fe-Ox	
74-79	713	528 ± 5	0.50	> 0.95	(Ad)+ Qtz + Cc + Fe-Ox	Charge & buffer capsules leaked
74-176	611	547 ± 5	0.20	0.20	Ad + Qtz + Cc + Fe-Ox	No reaction
74-173	611	550 ± 5	0.31	0.23	(Ad)+ Qtz + Cc + Fe-Ox	
74-169	612	560 ± 3	0.20	0.20	Ad + (Qtz + Cc + Fe-Ox)	
74-71	755	566 ± 7	0.50	0.50	(Ad)+ Qtz + Cc + Fe-Ox	
74-171	612	570 ± 5	0.21	0.23	Ad + (Qtz + Cc + Fe-Ox)	
74-69	755	577 ± 5	0.19	0.19	Ad + (Qtz + Cc + Fe-Ox)	
74-95	635	589 ± 5	0.50	0.48	(Ad)+ Qtz + Cc + Fe-Ox	
74-91	635	600 ± 3	0.50	0.54	Ad + (Qtz + Cc + Fe-Ox)	
74-99*	612	618 ± 3	0.50	0.24	Ad + Qtz + Cc + Fe-Ox	Charge leaked to buffer
74-97*	626	620 ± 5	0.50	> 0.95	(Ad)+ Qtz + Cc + Fe-Ox	Charge & buffer capsules leaked
74-96*	626	627 ± 3	0.50	0.29	Ad + (Qtz + Cc + Fe-Ox)	Charge leaked to buffer
SM-2	1335	639 ± 5	∿ 1.0	∿ 1.0	Ad + Qtz + Cc + Fe-Ox	No reaction; pure CO_2 plus one drop H_2O
SM-1	1335	649 ± 5	∿ 1.0	∿ 1.0	Ad + (Qtz + Cc + Fe-Ox)	Pure CO_2 plus one drop H_2O

†Condensed phases which were decreased in relative abundance during experiment are enclosed in brackets.
*Run experiments with buffer and/or charge capsules leaked.

slope of the reaction at $X_{CO_2} \leq 0.2$ suggests that andradite may be stable at temperatures as low as 250–350°C at P_{fluid} = 2000 bars.

Four runs of Gustafson (1971), with f_{O_2} defined by the NNO buffer, are also plotted in Figure 2 for comparison with our data. From his results and our experimentally-determined equilibrium boundary, the low-temperature stability of andradite is raised a maximum of about 25°C when f_{O_2} is lowered from that defined by the HM buffer to that defined by the NNO buffer. Calculations discussed below indicate a slightly larger temperature increase, on the order of 30°C at X_{CO_2} = 0.5.

Shoji (1975, p. 755) reported a few data on the synthesis of the grandite garnet series from oxide mixtures in increments of 20 X_{Ad} in unbuffered runs using pure H_2O and C–O–H fluids. Each grandite garnet was synthesized from a mixture of its own bulk composition only at temperatures above 500°C, P_{fluid} = 1000 bars, and with fluid compositions corresponding to X_{CO_2} = 0.17 and 0.25. Shoji did not report synthesis of any solid phases in experiments below 500°C, although, as noted below, andradite should be stable at 1000 bars and X_{CO_2} = 0.17 and 0.25 above 410° and 430°C, respectively.

Data for runs lying close to the equilibrium curve for reaction (1) are plotted in a log K *vs.* $10^3/T°(K)$ diagram in Figure 3, using fugacity coefficients for

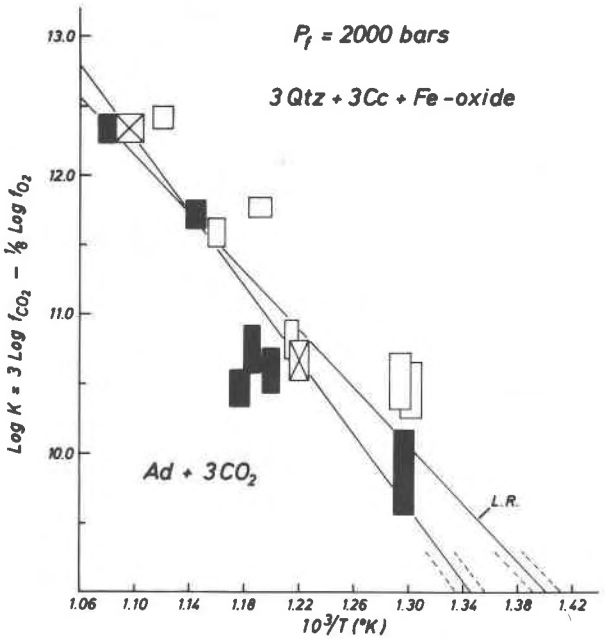

Fig. 3. Pertinent experimental data for the reaction 3 Qtz + 3 Cc + ¼ Hm + ½ Mt + ⅛ O_2 = Ad + 3 CO_2. Open rectangles indicate breakdown of andradite to quartz, calcite, and iron oxide. Solid rectangles indicate synthesis of andradite. Open rectangles with an "X" signify no reaction. In all cases, the size of the rectangle corresponds to experimental uncertainty. Data for runs lying far removed from the equilibrium are not plotted for the sake of clarity. L.R. = linear regression fit to the data, the other line is a subjective ("eye-ball") fit.

CO_2 from Burnham and Wall (personal communication, 1974) and values of f_{O_2} calculated from the modified equation for the HM buffer (Eugster and Wones, 1962; Huebner, 1971). Two straight lines, one a linear regression fit (L.R.) and the other a subjective ("eye-ball") fit, were plotted to describe the equilibrium. The equations of these lines are, respectively, $\log K^{2000} = -10.413\ (T^{-1}) + 23.60$ for the L.R., and $\log K^{2000} = -13.240\ (T^{-1}) + 26.84$ for the subjective fit. Comparison of the "goodness of fit" of these two lines and consideration of the experimental data suggest that a curved line, convex to both axes, would provide the best fit, implying that the enthalpy of reaction changes within the range of experimental conditions. Since the experiments plotted in Figure 3 were conducted at constant $P_{fluid} = P_{total}$, curvature of the equilibrium curve cannot be due to pressure-volume effects (see Orville and Greenwood, 1965). Skippen (1971, Fig. 7) found a curved line to best fit experimental data for a forsterite-producing decarbonation reaction.

A discrepancy exists between the standard enthalpy of reaction (ΔH_r^0) for reaction (1) calculated from data in Table 4 and from Robie and Waldbaum (1968) and that derived using equations for $\log K^{2000}$. The value of ΔH_r^0 derived from these tabulated thermodynamic data is 41.56 ± 5 kcal, which is considerably larger than the values of 24.35 or 26.31 kcal respectively from the L.R. and subjective fits to the experimental data in Figure 3. French (1971) noted an even larger discrepancy between calculated values of ΔH_r^0 and those values derived from a $\log K$ *vs.* $10^3/T$ plot for reactions describing the stability of siderite in the system Fe–C–O. French attributed the discrepancies to uncertainties in experimental and thermodynamic data. An additional possibility for the discrepancy in ΔH_r^0 for reaction (1) is that the enthalpy of reaction varies markedly with temperature.

The above expressions for $\log K^{2000}$ for reaction (1) serve, at best, to describe the equilibrium for the experimental conditions. These expressions may be useful when combined with similar $\log K$ expressions for other equilibria at 2000 bars (*e.g.*, see Skippen, 1971), but should not be used to calculate thermodynamic data at standard conditions. The results of calculations using more precise methods are given below.

Discussion

Thermodynamic data for andradite and hedenbergite

Reversed isobaric T–X_{CO_2} brackets for reaction (1) of this study and f_{O_2}–T brackets for reaction (2) involving Ad–Wol–Mt of Gustafson (1974) defining the high-temperature stability of andradite provide a basis for calculating thermodynamic data for andradite. The method of calculation used here follows that of Fisher and Zen (1971) and Zen (1973). Thermodynamic data for solid phases other than andradite and hedenbergite, as well as for CO_2, were taken from Robie and Waldbaum (1968), fugacity coefficients were from Burnham and Wall (personal communication, 1974), and data for H_2 were from Shaw and Wones (1964), and for H_2O from Fisher and Zen (1971) and Burnham *et al.* (1969). Calculations were made with the assumptions that solid phases participating in the reactions are pure and that H_2–H_2O and H_2O–CO_2 approximate ideal mixtures at the conditions of interest. The results are listed in Table 4.

The standard free energy of formation of andradite ($G_{f,Ad}^0$), derived by averaging the free-energy values calculated for each of the three closely-bracketed experimental points for reaction (1), is −1293.44 ± 1.2 kcal/gfw. A nearly identical value is obtained for $G_{f,Ad}^0$ when calculated assuming the reaction 3 Qtz +3

Table 4. Thermodynamic data for andradite and hedenbergite*

	V cal/bar	S° gb/gfw	ΔS_f° gb/gfw	S°** gb/gfw	ΔG_f° (Kcal/gfw)	ΔH_f° (Kcal/gfw)	Reaction used
Andradite (HM)	3.158			69.0	- 1293.44 ± 1.2	- 1377.48 ± 1.2	(1)
Andradite (HM)	"			"	- 1300.0 ± 1.9	- 1384.0 ± 2.0†	(2)
Andradite (NNO)	"	68.2 ± 3	- 282 ± 3	"	- 1301.1 ± 0.5	- 1385.1 ± 0.5	(3)
Andradite (QFM)	"	66.3 ± 3	- 284 ± 3	"	- 1303.2 ± 0.5	- 1387.8 ± 0.5	(3)
Hedenbergite (NNO)	1.625	36.0 ± 5	- 133 ± 5††	40.1	- 636.06# - 639.89##	- 675.91 - 679.73	(5)
	"	39.0 ± 5	- 133 ± 5	"	- 638.29# - 640.84##	- 677.75 - 680.30	(4)
Hedenbergite (QFM)	"	34.0 ± 5	- 137 ± 5	"	- 635.15# - 640.03##	- 676.09 - 680.97	(5)
Andradite (average)	3.158	67.3	-283	69.0	- 1297.80	- 1382.13	(1) (3)
Hedenbergite (average)	1.625	36.3	-134	40.1	- 638.44	- 678.58	(4) (5)

Reaction (1) $3SiO_2 + 3CaCO_3 + 1/4\ Fe_2O_3 + 1/2\ Fe_3O_4 + 1/8\ O_2 = Ca_3Fe_2Si_3O_{12} + 3CO_2$ (this paper)

(2) $Ca_3Al_2Si_3O_{12} + Fe_2O_3 = Ca_3Fe_2Si_3O_{12} + Al_2O_3$ (W. P. Nash and M. T. Einaudi, personal communication, 1975)

(3) $Ca_3Fe_2Si_3O_{12} = 3CaSiO_3 + 2/3\ Fe_3O_4 + 1/6\ O_2$ (Gustafson, 1974)

(4) $3\ Ca_3Fe_2Si_3O_{12} + 9SiO_2 + Fe_3O_4 = 9CaFeSi_2O_6 + 2\ O_2$ (Gustafson, 1974)

(5) $Ca_3Fe_2Si_3O_{12} + 2SiO_2 = 2CaFeSi_2O_6 + CaSiO_3 + 1/2\ O_2$ (Liou, 1974)

* Calculated using the methods of Fisher and Zen (1971) and Zen (1973).
** Third law entropy from the sum of oxides (Fyfe et al., 1958).
† Calculated from data of Robie and Waldbaum (1968) for the exchange reaction Grossular + Hematite = andradite + corundum (W. P. Nash & M. T. Einaudi, personal communication, 1975).
†† Compared to - 132 ± 5 derived from data in Robie and Waldbaum (1968) plus third law entropy from some oxides.
# Calculated using $\Delta G_{f,Ad}^\circ = -1293.44$
Calculated using $\Delta G_{f,Ad}^\circ = -1301.1$.

Cc + Hm = Ad + 3 CO_2 and the previously given experimental brackets, as must be the case for experimental temperatures and pressures along the HM buffer curve. Data from Gustafson (1974) on reaction (3) yield values of $G_{f,Ad}^0 = -1301.1 \pm 0.5$ and -1303.2 ± 0.5, respectively, for oxygen fugacities controlled by NNO and QFM buffers. The value of -1300 kcal/gfw obtained by W. P. Nash and M. T. Einaudi (personal communication, 1975) for the theoretical exchange reaction Gr + Hm = Ad + corundum is in good agreement with the $G_{f,Ad}^0$ calculated from Gustafson's data.

The reasons for the difference in values of $G_{f,Ad}^0$ derived from reactions (1) and (3) are not immediately obvious. The accuracy in determination of fluid composition constitutes an additional factor in the experimental uncertainty of each data point in our experiments, but cannot explain such a large difference in the $G_{f,Ad}^0$ values. The most likely explanation is the effect on the Gibbs free energy of andradite of substitution of Fe^{2+} for Ca^{2+} in the garnet structure. Cell dimensions of synthetic andradite measured by Gustafson (1974, p. 463) do show a decrease for andradite synthesized from starting materials with more reduced oxidation states, compatible with a proportionate increase in substituting Fe^{2+}. Increasing substitution of Fe^{2+} in andradite should increase the upper thermal stability of the garnet at fixed f_{O_2}, resulting in a correspondingly more negative calculated value for $G_{f,Ad}^0$. This possibility is in accord with the differences in $G_{f,Ad}^0$ given in Table 4 for reaction (3) conducted at NNO and QFM oxygen fugacities,

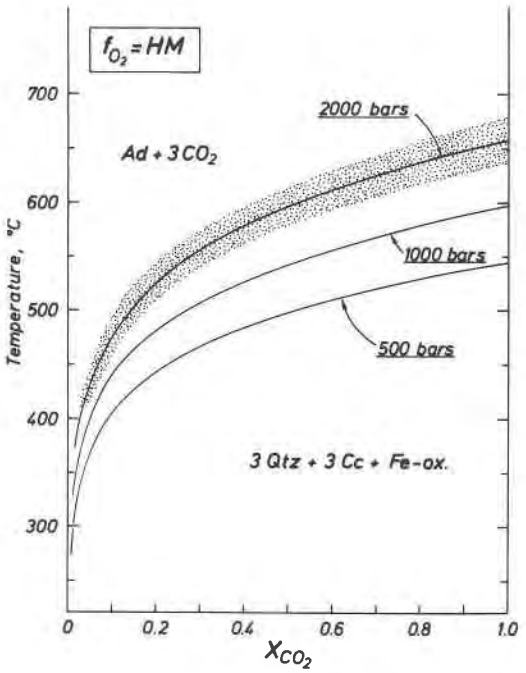

Fig. 4. T–X_{CO_2} diagram showing calculated curves at 2000, 1000, and 500 bars for the reaction 3 Qtz + 3 Cc + ¼ Hm + ½ Mt + ⅛ O_2 = Ad + 3CO_2 at f_{O_2} defined by the HM buffer. The uncertainty in X_{CO_2} and T due to the uncertainty in the calculated value of $G^0_{f,Ad}$ from the experimental data is shown by the stippled area for the 2000 bar curve; the experimental curve falls completely within the stippled area. The total uncertainty in T and X_{CO_2} for each calculated curve is somewhat larger, however, due to the uncertainty in thermodynamic data for other phases involved.

assuming relatively larger amounts of Fe^{2+} in andradite at lower f_{O_2}. The mean value of $G^0_{f,Ad}$ derived from experiments at oxygen fugacities of the HM, NNO, and QFM buffers is −1297.80 kcal/gfw.

Using the free energies of formation derived from reactions (1) and (3), plus available thermochemical data for wollastonite, quartz, and magnetite, we calculated the standard free energy of formation of hedenbergite ($G^0_{f,Hd}$) from the experimental data of Gustafson (1974) for reaction (4) involving Ad–Qtz–Hd–Wol. The $G^0_{f,Hd}$ values (Table 4) derived using the $G^0_{f,Ad}$ values from Gustafson's reaction (3) are about 2–4 kcal more negative that those $G^0_{f,Hd}$ values calculated with our $G^0_{f,Ad}$ from reaction (1), but are closer to a −643.34 kcal/gfw calculated by Kurshakova and Avetisyan (1974), based on their determination of reaction (5) (see also Kurshakova, 1971; Navrotsky and Coons, 1976). The mean value of $G^0_{f,Hd}$ is −638.44 kcal/gfw.

The entropies of formation of andradite and hedenbergite were also calculated from experimental data of Liou (1974) and Gustafson (1974) and from data in Robie and Waldbaum (1968). The calculated Third Law entropies (Fyfe *et al.*, 1958) of andradite and hedenbergite are 69.0 and 40.1 cal/deg-mole, respectively. From the entropy and free-energy data given in Table 4, the mean standard enthalpies of formation of andradite ($H^0_{f,Ad}$) and hedenbergite ($H^0_{f,Hd}$) are −1382.13 kcal/gfw and −678.59 kcal/gfw, respectively. The uncertainties listed in Table 4 are standard errors calculated according to the method suggested by Zen (1973).

Calculated T–X_{CO_2} relations for andradite and grandite garnets

Using the calculated thermodynamic data for andradite and hedenbergite listed in Table 4, we have computed the isobaric T–X_{CO_2} relations for reaction (1) for total pressures of 2000, 1000, and 500 bars, and the results are plotted in Figure 4. Thermochemical data for condensed phases and fugacity coefficients for CO_2 at 1000 to 2000 and at 500 bars were taken from Robie and Waldbaum (1968), Burnham and Wall (personal communication, 1974), and Mel'nik (1972), respectively. The stippled area shown

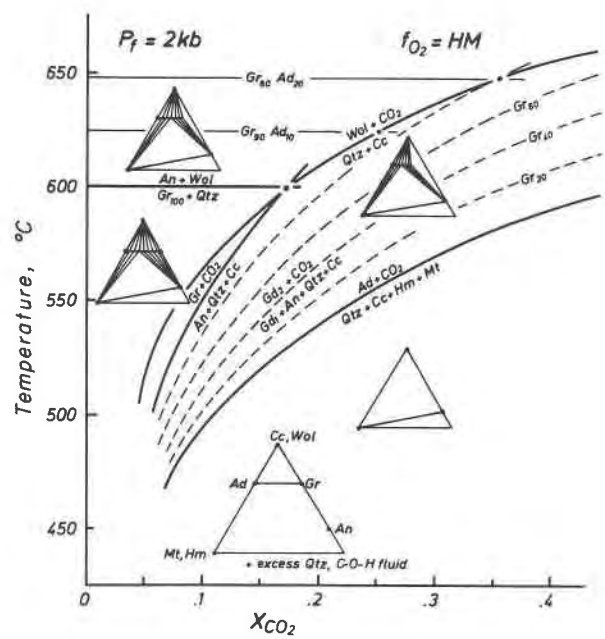

Fig. 5. T–X_{CO_2} diagram comparing the stability limits of grossular and andradite. The equilibria involving An–Qtz–Cc–Gr (7) and Qtz–Cc–Wol (6) are from Gordon and Greenwood (1971) and Greenwood (1967), respectively. The reaction Gr_{100} + Qtz = An + Wol (8) is from Newton (1966), and the temperatures of this reaction with addition of Fe^{3+} to grossular were calculated as discussed in text. Reactions involving two grandite garnets are shown by dashed lines in increments of 0.20 mole fraction of the garnet end members.

in Figure 4 for the equilibrium at 2000 bars represents the uncertainty in T and X_{CO_2} for the reaction due only to variation in the calculated free energies of formation of andradite from the three closely-bracketed experimental points given earlier; the experimental curve falls within the stippled area. The effect of total pressure on the equilibrium temperature at $X_{CO_2} = 0.5$ is about 55°C/1000 bars.

Experimentally determined isobaric T–X_{CO_2} relations for andradite and grossular are plotted in Figure 5 for comparison. The equilibrium curve for reaction (1) is taken from the present study and that for reaction (7) involving An–Qtz–Cc–Gr is from Gordon and Greenwood (1971). Also shown in Figure 5 are the equilibrium curves for reaction (6) from Greenwood (1967a) and for reaction (8) involving Gr–Qtz–An–Wol from Newton (1966). It is evident from the figure that the introduction of the andradite component into the grossular garnet decreases the temperature of formation for grandite garnet and expands the stability field for grandite + quartz toward both higher and lower temperatures as well as to more CO_2-rich environments. The variation in equilibrium temperature with varying garnet composition is contoured in Figure 5.

The variation in temperature of reaction (8) (Table 2) at 2000 bars with the addition of andradite to grossular garnet, *i.e.*, with the substitution of Fe^{3+} for Al, was calculated using the relation:

$$\ln K^{2000} = -2 \ln X_{Gr} = \frac{\Delta H_r^0}{RT} + \frac{\Delta S_r^0}{R} - \frac{\Delta V_r^0\,(1999)}{RT}$$

where X_{Gr} is the mole fraction of grossular in the grandite garnet, R is the gas constant, and ΔH_r^0, ΔS_r^0, and ΔV_r^0 are the standard enthalpy, entropy, and volume changes of reaction, respectively. The grandite garnet solution was assumed to be ideal, and the activity of each of the other mineral phases was taken as one.

The divariant curves for decarbonation reactions involving grandite garnet solutions shown in Figure 5 were drawn on the basis of the locations of the invariant point involving anorthite, wollastonite, grossular, quartz, and calcite, and the positions of the andradite- and grossular-forming decarbonation reactions. The compositions of the grandite garnets stable within the T–X_{CO_2} field between reactions (1) and (7) may be described by reactions of the type:

$$Gr_{90} + An + Qz + Cc + 1/2\ O_2 = 2\ Gr_{80} + CO_2,$$

which are also functions of f_{O_2}.

T–X_{CO_2} relations among other phases

With decreasing f_{O_2}, the stability limit of andradite in quartz-bearing calcareous rocks is significantly decreased and hedenbergite may become an important phase, as experimentally demonstrated by Gustafson (1974) and Liou (1974). An isobaric T–X_{CO_2} diagram at constant P_{fluid} = 2000 bars and at fixed f_{O_2} of $10^{-18.5}$ bars is constructed in Figure 6 to illustrate the low-temperature stability relations of andradite and hedenbergite, as well as several other calc-silicate equilibria pertinent to the formation of Ca–Al–Fe–Si skarns. For simplicity, several reactions at low values of T and X_{CO_2} have been omitted. Ideal mixing of H_2O and CO_2 was assumed. At this value of f_{O_2}, many reactions which involve andradite and/or hedenbergite, and which take place below the temperature of the graphite boundary, may still be conveniently shown, whereas at values of f_{O_2} less than $10^{-18.5}$ bars the stability field of andradite shrinks rapidly and the temperature of the graphite boundary decreases. Similarly, at values of f_{O_2} higher than $10^{-18.5}$ bars, the Hm–Mt boundary is raised to higher temperatures, modifying the phase relations of Fe-bearing phases. The position of the graphite boundary in Figure 6 was calculated from data given in Skippen (1971), and the temperature of the Hm–Mt boundary was calculated from a modified expression for the HM buffer (Eugster and Wones, 1962) given in Huebner (1971).

The positions of equilibria involving Ad–Qtz–Cc–Mt and Ad–Qtz–Cc–Hm in Figure 6 were calculated assuming a $G_{f,Ad}^0$ of −1293.44 kcal/gfw. The location of the decarbonation equilibrium involving Hd–Qtz–Cc–Mt was calculated assuming a $G_{f,Hd}^0$ of −638.44 kcal/gfw. Other data necessary to the calculations were taken from Robie and Waldbaum (1968) and Burnham and Wall (personal communication, 1974). Reaction (4) involving Ad–Qtz–Mt–Hd was experimentally determined by Gustafson (1974). The hedenbergite- and andradite-forming decarbonation reactions, (9) and (11), and reaction (4) intersect at invariant point C, from which radiates another reaction, (10), that involves Hd–Cc–Ad–Qtz and defines the CO_2-richest fluids with which andradite plus quartz is stable. Invariant points C and B are located, respectively, at T = 585°C, X_{CO_2} = 0.26, and T = 680 ± 10°C, X_{CO_2} = 0.31 ± 0.05. The error limits in T and X_{CO_2} for invariant point C can at present only be approximated. Gustafson (1974, p. 480) reports an uncertainty of 60°C in the intersection of reaction (4) with the NNO oxygen buffer curve; hence, 60°C must also be accepted as the *maximum* uncertainty in the

temperature of point C. The uncertainty in X_{CO_2} could then be as large as 0.075. Note that the slope of reaction (10) is controlled by the relative positions of invariant points B and C. Hence, the slope of reaction (10) changes rapidly with slight variations in f_{O_2}.

Well-determined equilibria in the Fe-free portion of the system represented by Figure 6 include reactions (6) Qtz–Cc–Wol (Greenwood, 1967a), (7) An–Qtz–Cc–Gr (Gordon and Greenwood, 1971), and (8) Gr–Qtz–An–Wol (Newton, 1966). These equilibria intersect at invariant point A, located at $T = 600 \pm 10$°C and $X_{CO_2} = 0.15 \pm 0.025$ (Gordon and Greenwood, 1971).

Clinozoisite (zoisite) and epidote may crystallize as a result of reactions between skarn and metasomatic fluid; hence a number of equilibria involving clinozoisite (zoisite) and epidote are also plotted in Figure 6. The T–X_{CO_2} locations of reaction (12) in which An + Gr form at the expense of Zo + Qtz and reaction (13) in which Gr forms from Zo + Qtz + Cc are from Gordon and Greenwood (1971). Reaction (14) involving Zo–An–Cc is plotted after the experimental data of Johannes and Orville (personal communication, 1974), with a somewhat steeper slope than that shown by Gordon and Greenwood (1971). Reactions (12), (13), and (14) define a clinozoisite (zoisite)-bearing invariant point E located at $T = 510$°C and $X_{CO_2} = 0.06$ (Gordon and Greenwood, 1971).

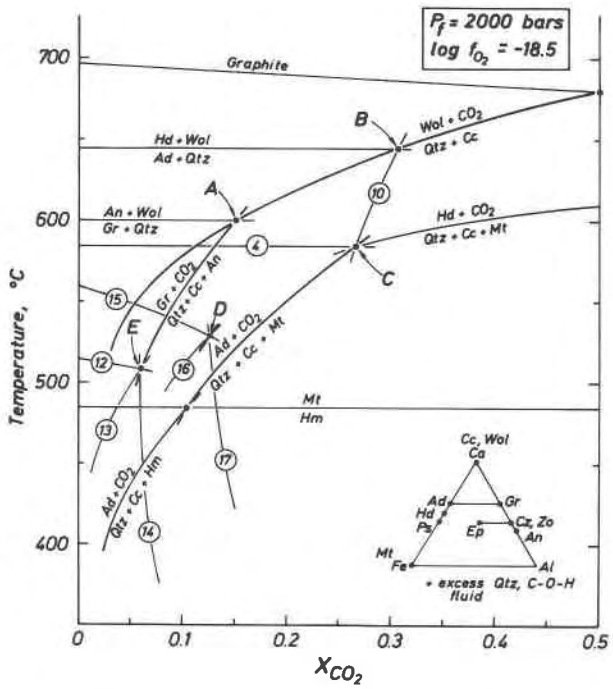

Fig. 6. T–X_{CO_2} diagram at $P_{fluid} = 2000$ bars for $\log f_{O_2} = -18.5$, *i.e.* slightly above the NNO buffer for the temperature range shown. Reactions (12)–(14) involve zoisite (clinozoisite) and reactions (15)–(17) epidote and are discussed in the text, along with invariant points A–D. Reaction (4) and the reaction involving Ad–Qtz–Hd–Wol were determined by Gustafson (1974) and Liou (1974), respectively. The Qtz–Cc–Wol, Gr–Qtz–An–Wol, and An–Qtz–C–Gr equilibria are from Greenwood (1967a), Newton (1966), and Gordon and Greenwood (1971), respectively. Zoisite-bearing reactions (12)–(14) are from Gordon and Greenwood (1971) and Johannes and Orville (personal communication, 1974). Reactions (15)–(17) involve epidote and are discussed in the text. The positions of the equilibria involving Ad–Qtz–Cc–Mt, Ad–Qtz–Cc–Hm, and Hd–Qtz–Cc–Hm were calculated using data in Table 4 (this paper), Robie and Waldbaum (1968), and Burnham and Wall (personal communication, 1974). The graphite boundary was located using data in Skippen (1971) and the Hm–Mt boundary from the expression for the HM buffer given in Huebner (1971).

Reactions (15), (16), and (17) in Figure 6 are epidote-bearing equilibria which are analogous, respectively, to zoisite-bearing reactions (12), (13), and (14) in the Fe-free portion of the system Ca–Al–Fe–Si–C–O–H. The epidote-bearing reactions are not explicitly balanced in Table 2 because the exact compositions of the epidote, grandite, and iron-oxide phase are not known. Experimental investigations of Holdaway (1972) and Liou (1973) suggest that the breakdown of epidote + quartz, reaction (15), results in a grandite garnet with a mole fraction of grossular approximately equal to the mole fraction of pistacite in the original epidote. The iron-oxide phase present in reaction (15) may actually be a magnetite–hercynite solution (Liou, 1973). Ps_{30} and Ad_{70} are assumed, respectively, for the compositions of epidote and grandite garnet in reactions (15), (16), and (17) plotted in Figure 6. These reactions radiate from invariant point D, which is located approximately at $T = 530$°C and $X_{CO_2} = 0.12$. Invariant point D lies along an equilibrium curve involving grandite with the composition $Ad_{70}Gr_{30}$ (see also Fig. 5). The effect of minor substitution of Fe^{2+} for Ca^{2+} in the grandite garnet on the temperature of this reaction has been ignored.

Figure 6 illustrates, therefore, the relative T–X_{CO_2} stability fields at $P_{fluid} = 2000$ bars for clinozoisite (zoisite), epidote, grossular, and andradite and the low-temperature stability limit of hedenbergite and wollastonite in the presence of excess quartz and with f_{O_2} of $10^{-18.5}$ bars, and is useful to interpret the effects of isobaric variations in T, X_{CO_2}, and f_{O_2} on calc-silicate equilibria in skarns. Comparison of the phase relations shown in Figures 5, 6, and 7 indicates that while the stability field of andradite plus quartz shrinks significantly with a slight decrease in f_{O_2}, the temperature of the upper stability limit of andradite is more drastically affected by variations in f_{O_2} than

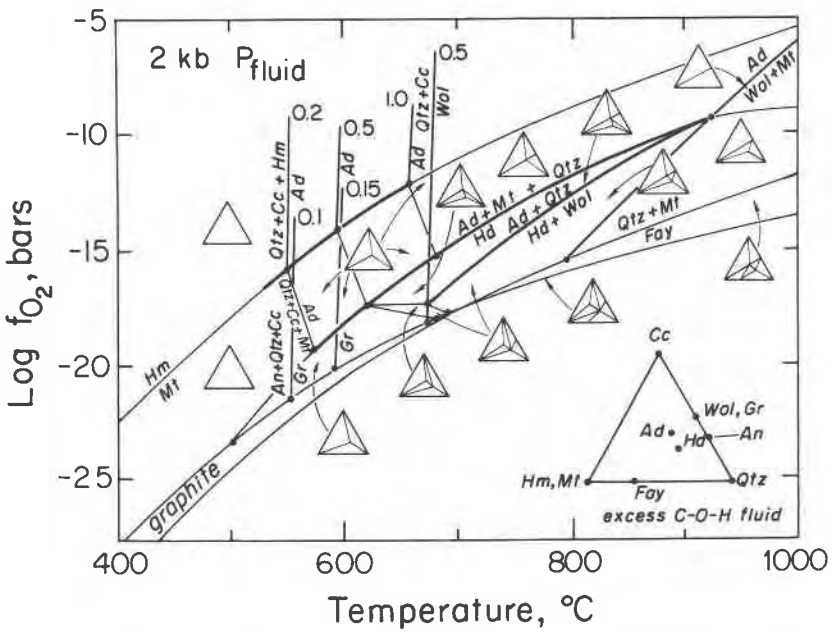

Fig. 7. Log f_O–T diagram for several reactions in the system Ca–Fe–Si–O–H (modified after Liou, 1974). Reaction (7), An + Qtz + Cc = Gr + CO_2 (Gordon and Greenwood, 1971), is shown for comparison with reaction (1), 3 Qtz + 3 Cc + FeOx = Ad + 3 CO_2. Mole fractions of CO_2 in C–O–H fluids are shown adjacent to garnet and wollastonite decarbonation reactions. Other reactions involving Gr and An, as well as several involving fayalite, are omitted for clarity. The slope for the reaction 3 Qtz + 3 Cc + ⅔ Mt + ½ O_2 = Ad + 3 CO_2 is estimated from reconnaissance data of Gustafson (1971; see text). The Qtz–Cc–Wol reaction is from Greenwood (1967a), the Hd–Ad–Qtz–Mt, Ad–Wol–Mt, and Hd–Wol–Mt equilibria are from Gustafson (1974), and the Ad–Qtz–Hd–Wol equilibrium is from Liou (1974). The positions of the buffer curves were plotted from equations summarized in Huebner (1971).

the X_{CO_2} limits of other limiting reactions for andradite.

With decrease in f_{O_2}, f_{CO_2} is also reduced, due to an increase in the relative proportions of CO and CH_4 formed by the reactions

$$CO_2 = CO + 1/2\ O_2$$

and

$$CO_2 + H_2 = 2\ H_2O + CH_4.$$

Accordingly, the X_{CO_2} limits of reactions involving H_2O and/or CO_2 will be shifted slightly relative to their positions as shown in Figure 6. Positive-slope decarbonation reactions would be shifted to slightly higher values of X_{CO_2}, and reactions (13) and (16), which also involve dehydration, to slightly lower values (see also Kerrick, 1974). In the absence of graphite (*i.e.* at temperatures below the graphite boundary for a given f_{O_2}), changes in positions of the reaction boundaries in a T–X_{CO_2} diagram are rather small, due to the minor abundances of CO and CH_4 (Eugster and Skippen, 1967)—H_2O and CO_2 constitute the principal fluid species (Greenwood, 1967b).

T–f_{O_2} relations

Isobaric T–log f_{O_2} relations at 2000 bars involving andradite and related phases in the system Ca–Fe–Si–C–O–H are shown in Figure 7. The upper thermal stability limits of andradite, andradite + quartz, and andradite + quartz + magnetite are from the experimental data of Gustafson (1974) and Liou (1974). Our experimental results for reaction (1) were plotted at X_{CO_2} = 1.0, 0.5, and 0.2 along the HM buffer curve. Each point represents the intersection of two reactions with the HM buffer curve, one with hematite and the other with magnetite as the only iron-oxide phase present. These points of intersection are shifted along the HM buffer curve to lower temperatures with decrease in X_{CO_2}.

In contrast to the reactions defining the upper thermal stability limits of andradite, andradite + quartz, and andradite + quartz + magnetite, the temperature of formation for andradite from quartz + calcite + magnetite shown in Figure 7 increases with decrease in x_{O_2} at constant P_{fluid}. The estimated temperature for the equilibrium Cc–Qtz–Mt–Ad at f_{O_2} of the NNO buffer and X_{CO_2} = 1.0 is plotted about 25°C higher than that of the reaction determined at f_{O_2}

defined by the HM buffer. The low-temperature stability limits of grossular as defined by reaction (7) at $X_{CO_2} = 0.1$ and 0.15 (Gordon and Greenwood, 1971) are also plotted in Figure 7 for comparison.

Petrologic applications

Our experimental results on reaction (1) shown in Figure 2 delineate the lowest temperature of formation of andradite. Many other calculated as well as experimentally determined equilibria shown in Figures 5, 6, and 7 may be used to characterize the T, X_{CO_2}, and f_{O_2} conditions for various mineral assemblages in natural Ca–Si–Fe–Al skarns. However, extreme caution should be taken in applying these data to interpret physico-chemical parameters in natural systems because (a) garnets of natural skarn are not pure end-members, (b) f_{O_2} values during the skarn formation are difficult to estimate, (c) other components, such as sulfur, may be significant in the metasomatic fluid, and (d) equilibrium between numerous phases in skarn-forming processes may not have been attained in many cases. Variation in garnet composition (*e.g.*, Fig. 3) and in f_{O_2} (*e.g.*, Fig. 7), and introduction of sulfur into the fluid phase would significantly modify the phase relations shown in Figures 5, 6, and 7 (Burt, 1972; Gamble, 1976). Nevertheless, the present study may be used to estimate temperature and fluid composition for grandite-bearing skarns in some instances as described below.

Experimental results indicate that andradite is restricted to only H_2O-rich fluid at temperatures below 400°C. Andradite in regional metamorphic rocks has been described from the prehnite–pumpellyite facies metavolcanic rocks in New Zealand (Coombs *et al.*, 1977) and from serpentinite from the Austroalpine Nappe in the Alps (Peters, 1965). Hematite was found associated with andradite in the New Zealand occurrence, and the depth of burial indicates a P_{fluid} of about 2 kbar, assuming $P_{total} = P_{fluid}$. From the data in Figure 2, we conclude that in the metamorphic fluid prevailing during the crystallization of andradite in the burial metamorphic rocks in New Zealand, X_{CO_2} must have been lower than 0.02. The lack of quartz and hematite in the andradite + calcite + magnetite + serpentine assemblage in the alpine serpentinite, as well as substitution of (OH) for Si in the hydroandradite prohibits a detailed comparison with our data, but the metamorphic fluid must have been very H_2O-rich (*i.e.*, $X_{CO_2} < 0.02$).

Scharbert (1966) described 3 cm thick zoned skarn layers in marble from the Bohemian Massif ("Buntner Serie" of the Moldanubian Zone). From the marble to the center of each layer, the mineral zonation consists of a hedenbergite zone followed by a grandite-rich core. Calcite is the dominant mineral in the marble, and wollastonite is notably absent. No epidote was found in the skarn. The grandite garnet was reported to have the composition $Ad_{80}Gr_{20}$; it contains inclusions of quartz and is associated with magnetite and calcite. If we assume the f_{O_2} during the formation of garnet to have been similar to that shown in Figure 6, then X_{CO_2} in the fluid phase present during the crystallization of andradite at the expense of quartz + calcite + magnetite in the core of the skarn must have been between 0.13 and 0.24. The presence of the hedenbergite zone and the absence of wollastonite in the marble suggest that the temperature during the formation of the skarn layers must have reached 580° to 600°C. A gradient in X_{CO_2}, decreasing from greater than 0.24 in the marble and hedenbergite zones to as low as 0.13 in the grandite-rich zone, may have been obtained.

In most metasomatic skarns associated with igneous intrusions, the replacement of andradite-rich garnet by quartz + calcite + iron oxide in a C–O–H fluid occurs primarily as a retrograde process. For example, scheelite-bearing skarns in the Marcus mine in the Osgood Mountains, Nevada, contain garnet and pyroxene as the most dominant phases (Taylor, 1976). Garnet in these skarns has the composition of $Ad_{90}Gr_{10}$, and most samples of skarn contain quartz, calcite, and hematite–magnetite as the principal retrograde minerals, along with trace amounts of epidote. Minor pyrite is associated with magnetite, and tremolitic amphibole replaces salitic pyroxene. The presence of intergrown hematite and magnetite and the pseudomorphic replacement of hematite by magnetite (Fig. 8A) suggest that f_{O_2} during the retrograde replacement was near that defined by the HM buffer. These retrograde mineral assemblages are in contrast to those found in skarns elsewhere around the Osgood Mountain granodiorite stock; the other skarns contain more aluminous garnet which was replaced by anorthite, epidote, and Fe-rich amphibole, and hematite is not present (Fig. 8B). Maximum confining pressure during metamorphism and metasomatism associated with the emplacement of the Osgood Mountain granodiorite was estimated by Taylor (1976) at approximately 1500 bars.

From the calculated T–X_{CO_2} curves for reaction (1) shown in Figure 4 and reaction temperature of 450°–550°C based on oxygen-isotope fractionations (Taylor, 1974; Taylor and O'Neil, 1977), the metasomatic fluids present in the skarns of the Marcus mine dur-

ing the retrograde replacement of garnet and pyroxene could have contained X_{CO_2} up to 0.2.

Addition of Al to the system permits the crystallization of Al–Fe grandite garnet, and mineral reactions involving the intermediate grandite garnets are more complex than those involving either pure grossular or andradite, as shown in Figure 5. Kerrick (1970) described several assemblages of calc-silicate minerals in rocks from roof pendants in the Sierra Nevada, California, which contained grandite garnet with a composition of $Gr_{90}Ad_{10}$. He found that the decomposition temperature of grandite garnet + quartz to anorthite + wollastonite increases due to the addition of Fe^{3+} to grossular. His suggestion is compatible with the increase in temperature of the grandite decomposition reaction with Fe content of the garnet shown in Figure 5.

Grandite garnet in Fe-rich metasomatic skarns may be replaced by mineral assemblages including calcic plagioclase, epidote, and amphibole in addition to quartz, calcite, and iron oxide. Fe-bearing sulfides may also form, depending on the f_{S_2} in the fluid, and sphene is often present as a replacement product of Ti-bearing garnet. Such skarn garnets are typically zoned with respect to Al and Fe, and certain zones in garnets of some skarns may be selectively replaced during retrograde reactions of the skarn with the metasomatic fluid. Selective replacement of zoned garnet has been described in skarns from the Sierra Nevada, for example by Brock (1972) and Morgan (1975). In the skarns from mines other than the Marcus in Osgood Mountains, Nevada (Taylor, 1976), Fe-rich zones of grandite garnets are characteristically replaced by epidote, whereas the Al-rich zones of the garnet are virtually unattacked. These reaction relationships may be explained by phase relations in Figure 6, which indicate that Fe-rich garnet is replaced by epidote in H_2O-rich fluids via reaction (15) at higher temperatures than the analogous reaction (12) involving Al-rich garnet. Hence, under falling temperatures, the retrograde replacement of andradite-rich garnet in skarns in the presence of H_2O-rich fluids is to be expected before the replacement of grossular-rich garnet.

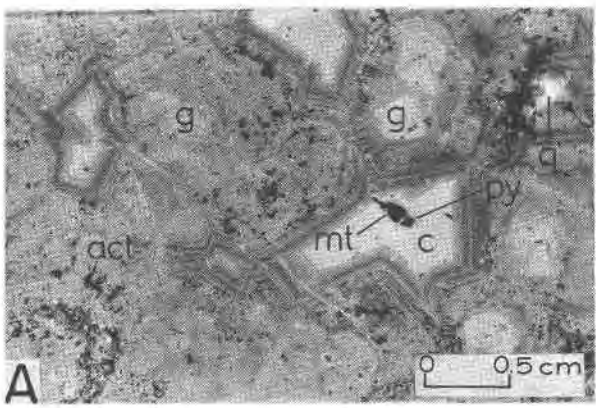

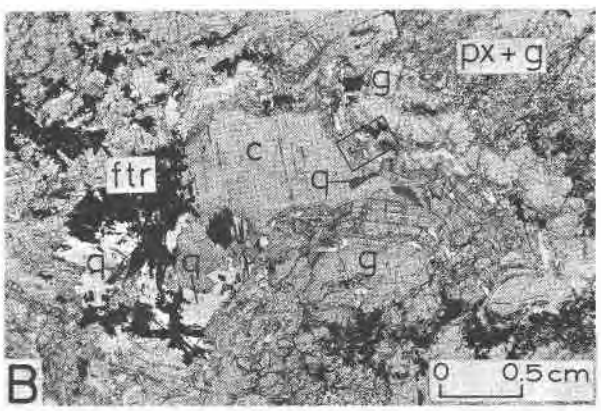

Fig. 8A. Photomicrograph of garnet–pyroxene skarn from the Marcus mine, Osgood Mountains, Nevada (sample 73-186-4; Taylor, 1976). The andradite-rich garnet has been partially replaced by the low-temperature assemblage quartz, magnetite, and calcite. Magnetite is pseudomorphic after hematite. Actinolitic amphibole has partially replaced pyroxene (plane polarized light).

Fig 8B. Photomicrograph of filled void in garnet–pyroxene skarn from Granite Creek mine, Osgood Mountains, Nevada (sample 72-60-2; Taylor, 1976). Note the paragenesis of pyroxene plus garnet (px + g) followed by garnet. Garnet and pyroxene were selectively replaced by ferrohastingsitic amphibole (ftr). Several Fe-rich zones in the garnet rim have been selectively replaced by quartz, calcite, and amphibole (plane polarized light).

Summary

The low-temperature stability limit of andradite in C–O–H fluids, which we have determined as a function of f_{O_2}, X_{CO_2}, T, and P_{fluid}, is an important boundary reaction in the system Ca–Al–Fe–Si–C–O–H. Together with other previously investigated reactions involving grossular, wollastonite, anorthite, quartz, and calcite in C–O–H fluids, the Ad–Qtz–Cc–Hm–Mt equilibrium described in this paper broadens our quantitative knowledge of the conditions of formation of Ca–Si–Fe–Al skarns. The stability field of Fe-bearing grandite in the presence of a C–O–H fluid is markedly enlarged over that for grossular with respect to both temperature and X_{CO_2} at fixed f_{O_2} and P_{fluid}. The upper temperature stability limit of andradite (plus quartz) is sensitive to slight variations in f_{O_2}, whereas the temperature of other reactions involving andradite are more sensitive to variations in X_{CO_2}. The breakdown of grandite to epidote-bearing

mineral assemblages in H_2O-rich fluids explains why the replacement of grandite garnet by a second garnet, anorthite, quartz, and calcite, or of andradite by quartz, calcite, and iron oxide is seldom observed in skarns.

Acknowledgments

Field work associated with this research was supported partially by the U.S. Geological Survey, and partially by Conoco Oil Company (courtesy of B. R. Berger). Discussions with M. T. Einaudi, Stanford University, regarding some aspects of phase relations involving garnet, and with K. Bucher-Nurminen, ETH, Zürich, regarding the thermodynamic calculations, were very helpful. We are also grateful for the financial support for this study provided by NSF Grant GA 37177/Liou and by a Geological Society of American Penrose Grant (1754–73) and a Sigma Xi Grant-in-Aid-of-Research (both to B. E. Taylor). This paper was prepared in its final form while Taylor was supported by an Alexander von Humboldt-Stiftung Fellowship at the University of Tübingen, Federal Republic of Germany. Comments by M. T. Einaudi and W. G. Ernst on an earlier draft of this manuscript and a perceptive review by D. Eggler are gratefully acknowledged.

References

Brock, K. J. (1972) Genesis of garnet skarn, Calaveras County, California. *Geol. Soc. Am. Bull., 83,* 3391–3404.

Burnham, C. W., J. R. Holloway, and N. F. Davis (1969) Thermodynamic properties of water to 1000°C and 10,000 bars. *Geol. Soc. Am. Spec. Paper 132.*

Burt, D. M. (1971a) Some phase equilibria in the system Ca–Fe–Si–C–O. *Carnegie Inst. Wash. Year Book, 70,* 178–184.

——— (1971b) The facies of some Ca–Fe–Si skarns in Japan. *Carnegie Inst. Wash. Year Book, 70,* 189–197.

——— (1971c) Multisystems analysis of the relative stabilities of babingtonite and ilvaite. *Carnegie Inst. Wash. Year Book, 70,* 185–188.

——— (1972) *Mineralogy and geochemistry of Ca–Fe–Si skarn deposits.* Ph. D. Thesis, Harvard University, Cambridge, Mass.

——— (1974) Metasomatic zoning in Ca–Fe–Si exoskarns. In A. W. Hofmann, B. J. Giletti, H. S. Yoder, Jr. and R. A. Yund, Eds., *Geochemical Transport and Kinetics,* p. 187–193. Carnegie Inst. Wash. Publ. 634.

Coombs, D. S., Y. Kawachi, B. F. Houghton, G. Hyden, I. J. Pringle, and J. G. Williams (1977) Andradite and andradite–grossular solid solutions in very low-grade regionally metamorphosed rocks in southern New Zealand. *Contrib. Mineral. Petrol, 63,* 229–246.

Eugster, H. P. (1957) Heterogeneous reactions involving oxidation and reduction at high temperature and pressure. *J. Chem. Phys., 26,* 1760–1761.

——— and G. B. Skippen (1967) Igneous and metamorphic reactions involving gas equilibria. In P. H. Abelson, Ed., *Researches in Geochemistry, II,* p. 492–520. John Wiley and Sons, New York.

——— and D. R. Wones (1962) Stability relations of the ferruginous biotite, annite. *J. Petrol., 3,* 82–125.

Fisher, J. R. and E-an Zen (1971) Thermodynamic calculations from hydrothermal phase equilibrium data and free energy of H_2O. *Am. J. Sci., 270,* 297–314.

French, B. M. (1971) Stability relations of siderite ($FeCO_3$) in the system Fe–C–O. *Am. J. Sci., 271,* 37–38.

Fyfe, W. S., F. J. Turner and J. Verhoogen (1958) Metamorphic reactions and metamorphic facies. *Geol. Soc. Am. Mem. 73.*

Gamble, R. P. (1976) The sulfidation of andradite and hedenbergite and the formation of skarn sulfides (abstr.). *Geol. Soc. Am. Abstracts with Programs, 8,* 879.

Gordon, T. M. and H. J. Greenwood (1971) The stability of grossularite in H_2O–CO_2 mixtures. *Am. Mineral., 56,* 1674–1688.

Greenwood, H. J. (1967a) Wollastonite: stability in H_2O–CO_2 mixtures and occurrence in a contact-metamorphic aureole near Salmo, British Columbia, Canada. *Am. Mineral., 52,* 1669–1680.

——— (1967b) Mineral equilibria in the system MgO–SiO_2–H_2O–CO_2. In P. H. Abelson, Ed., *Researches in Geochemistry, II,* p. 542–567. John Wiley and Sons, New York.

Gustafson, W. L. (1971) *Stability Relations of Andradite, Hedenbergite, and Related Minerals in the System Ca–Fe–Si–O–H.* Ph.D. Thesis, University of California, Los Angeles.

——— (1974) The stability of andradite, hedenbergite, and related minerals in the system Ca–Fe–Si–O–H. *J. Petrol., 15,* 455–496.

Harker, R. I. and O. F. Tuttle (1955) Studies in the system CaO–MgO–CO_2, 1. The thermal dissociation of calcite, dolomite, and magnetite. *Am. J. Sci., 253,* 209–224.

Holdaway, M. J. (1972) Thermal stability of Al–Fe epidote as a function of f_{O_2} and Fe content. *Contrib. Mineral. Petrol., 37,* 307–340.

Holloway, J. R., C. W. Burnham and G. L. Millhollen (1968) Generation of H_2O–CO_2 mixtures for use in hydrothermal experimentation. *J. Geophys. Res., 73,* 6598–6600.

Huckenholz, H. G. and H. S. Yoder (1971) Andradite stability relations in the $CaSiO_3$–Fe_2O_3 join up to 30 kb. *Neues Jahrb. Mineral. Abh., 114,* 246–280.

Huebner, J. S. (1971) Buffering techniques for hydrostatic systems at elevated pressures. In G. C. Ulmer, Ed., *Research Techniques for High Pressure and High Temperature,* p. 123–176. Springer-Verlag, Heidelberg.

Kerr, P. F. (1946) Tungsten mineralization in the United States. *Geol. Soc. Am. Mem., 15,* 241 p.

Kerrick, D. M. (1970) Contact metamorphism in some areas of the Sierra Nevada, California. *Geol. Soc. Am. Bull., 81,* 2913–2938.

——— (1974) Review of metamorphic mixed-volatile (H_2O–CO_2) equilibria. *Am. Mineral., 59,* 729–762.

Kurshakova, L. D. (1968) Redox conditions for the andraditization of hedenbergite. In *Theoretical and experimental investigations of mineral equilibria.* Nauka Press, Moscow.

——— (1970) Experimental study of the hedenbergite + wollastonite = andradite + quartz reaction. *Ocherki Fiz. Khim. Petrol., 2,* 99–115.

——— (1971) Effect of oxygen fugacity on the stability of hedenbergite and andradite in the system Ca–Fe–Si–O_2. *Ocherki Fiz. Khim. Petrol., 3,* 49–60.

——— and E. I. Avetisyan (1974) Stability and properties of synthetic hedenbergite. *Geochem. Int., 11,* 444–453.

Liou, J. G. (1973) Synthesis and stability of epidote, $Ca_2Al_2FeSi_3O_{12}(OH)$. *J. Petrol., 14,* 381–413.

——— (1974) Stability relations of andradite–quartz in the system Ca–Fe–Si–O–H. *Am. Mineral., 59,* 1016–1025.

Luth, W. C. and C. O. Ingamells (1965) Gel preparation for starting materials for hydrothermal experimentation. *Am. Mineral., 50,* 255–258.

Mel'nik, Yu. P. (1972) Thermodynamic parameters of compressed gases and metamorphic reactions involving water and carbon dioxide. *Geochem. Int., 9,* 1–13.

Morgan, B. A. (1975) Mineralogy and origin of skarns in the

Mount Morrison Pendant, Sierra Nevada, California. *Am. J. Sci., 275,* 119–142.

Navrotsky, A. and W. E. Coons (1976) Thermochemistry of some pyroxenes and related compounds. *Geochim. Cosmochim. Acta, 40,* 1281–1288.

Newton, R. C. (1966) Some calc-silicate equilibrium relations. *Am. J. Sci., 264,* 204–222.

Orville, P. M. and H. J. Greenwood (1965) Determination of ΔH of reaction from experimental pressure-temperature curves. *Am. J. Sci., 263,* 678–683.

Peters, Tj. (1965) A water-bearing andradite from the Totalp serpentine (Davos, Switzerland). *Am. Mineral., 50,* 1482–1486.

Robie, R. A. and D. R. Waldbaum (1968) Thermodynamic properties of minerals and related substances at 298.15°K (25°C) and one atmosphere (1.013 bars) pressure and at higher temperatures. *U.S. Geol. Surv. Bull. 1259.*

Scharbert, H. G. (1966) Andradite-führende Einschaltungen im Marmor von Hartenstein (Kl, Kremstal, N. Ö.). *Neues Jahrb. Mineral. Monatsh., 221–223.*

Shaw, H. R. (1963) Hydrogen–water vapor mixtures: control of hydrothermal atmospheres by hydrogen osmosis. *Science, 139,* 1220–1222.

——— and D. R. Wones (1964) Fugacity coefficients for hydrogen gas between 0° and 1000°C for pressures to 3000 atm. *Am. J. Sci., 262,* 918–929.

Shoji, T. (1975) Role of temperature and CO_2 pressure in the formation of skarn and its bearing on mineralization. *Econ. Geol., 70,* 739–749.

Skippen, G. B. (1971) Experimental data for reactions in siliceous marbles. *J. Geol., 79,* 457–481.

Taylor, B. E. (1974) Communication between magmatic and meteoric fluids during formation of Fe-rich skarns in north-central Nevada (abstr.). *Trans. Am. Geophys. Union., 54,* 478.

——— (1976) *Origin and Significance of C–O–H Fluids in the Formation of Ca–Fe–Si Skarn, Osgood Mountains, Humboldt County, Nevada.* Ph.D. Thesis, Stanford University, Stanford, California.

——— and J. R. O'Neil (1977) Stable isotope studies of metasomatic Ca–Fe–Al–Si skarns and associated metamorphic and igneous rocks, Osgood Mountains, Nevada. *Contrib. Mineral. Petrol., 63,* 1–49.

Zen, E-an (1973) Thermochemical parameters of minerals from oxygen-buffered hydrothermal equilibrium data: method, application to annite and to almandine. *Contrib. Mineral. Petrol., 39,* 65–80.

Manuscript received, April 13, 1977; accepted for publication, October 12, 1977.